Applied Catalysis B: Environmental 237 (2018) 513–520

Contents lists available at ScienceDirect

Applied Catalysis B: Environmental

journal homepage: www.elsevier.com/locate/apcatb

FeOOH quantum dots coupled g-C_3N_4 for visible light driving photo- Fenton degradation of organic pollutants

Xufang Qian[a], Yunwen Wu[a], Miao Kan[a], Mengyuan Fang[a], Dongting Yue[a], Jun Zeng[b], Yixin Zhao[a,*]

[a] School of Environmental Science and Engineering, Shanghai Jiao Tong University, 800 Dongchuan Road, Shanghai, 200240, China
[b] Key Laboratory of Green Chemistry of Sichuan Institutes of Higher Education, Sichuan University of Science & Engineering, China

ARTICLE INFO

Keywords:
FeOOH QD
g-C_3N_4
Visible light driving
Photo-Fenton
Organic pollutants

ABSTRACT

Amorphous FeOOH quantum dots (QDs) were coupled with polymeric photocatalysts g-C_3N_4 which was developed as a visible light driving photo-Fenton catalyst. Highly dispersed FeOOH QDs anchored on g-C_3N_4 showed enhanced visible light driving photo-Fenton degradation of MO and phenol than that of pure g-C_3N_4 and mechanical mixture (FeOOH&g-C_3N_4). The mineralization efficiency on FeOOH/g-C_3N_4 is nearly 7 times higher than that on pure g-C_3N_4 which shows great potential in treatment of recalcitrant organic pollutants. XPS results indicated that extraneous carbon species were present in FeOOH/g-C_3N_4 which should be responsible for the electron transfer between FeOOH and g-C_3N_4. Based on the radical capture, electrochemical experiments and photoluminescence (PL) decay characterizations, we proposed that visible light excited the g-C_3N_4 to produce e^-/h^+ pairs and the e^- participated the cycling of Fe(II)/Fe(III). The FeOOH/g-C_3N_4 showed high recycling stability without Fe leaching due to the interaction of FeOOH QDs and carbon species. The FeOOH QDs coupled g-C_3N_4 is a promising visible light driving photo-Fenton catalyst for organic pollutants treatment.

1. Introduction

The rapid development of industrialization caused serious damage to the living environment. In particular, the discharge of various pollutants and by-products in the process of industrial production makes the water, air and soil overloaded [1,2]. For homogeneous Fe^{2+}/H_2O_2 Fenton reaction, the soluble Fe^{2+} catalyzed hydrogen peroxide reaction to produce hydroxyl radical with strong oxidation ability (·OH, oxidation potential of 2.80 V) [3]. But the traditional homogeneous catalyst has the following shortcomings: 1) limited Fenton activity and low utilization efficiency of hydrogen peroxide; 2) wastewater discharge with high iron content (50–80 ppm), severely exceeding the discharge standard of water in China and EU (2 ppm); 3) sludge residue contains large amounts of iron species; 4) optimal pH around 2.5–3.5 consuming lots of acid; 5) presence of organic complex agents reducing the Fenton activity of Fe^{2+} [4–6].

In recent years, heterogeneous photo- and Fenton-catalysis has been widely studied as the environmentally friendly method to degrade organic pollutants in water and soil [7–11]. Zhang et al. classified heterogeneous Fenton systems into heterogeneous Fenton-like and surface Fenton ones [12]. The former inevitably resulted in soluble iron ions and homogeneous Fenton reaction to some extent, while surface Fenton reaction normally proceeded on the surface of catalysts without iron leaching. Iron-based heterogeneous catalysts were widely studied due to its merits of high natural abundance, low cost, low toxicity and environmental friendly properties [13–19]. However, the efficiency of heterogeneous iron-based Fenton catalysts is generally low due to the limited exposed iron active sites and the slow cycling of Fe(III) /Fe(II) during heterogeneous Fenton reaction [20,21]. The iron leaching also was serious in acidic aquatic environment. g-C_3N_4 has recently emerged as a promising visible light responsive photocatalyst for water purification and H_2 production [22]. Wang et al also found that the visible light excited of g-C_3N_4 catalyzed H_2O_2 to produce ·OH [23]. g-C_3N_4 combined with different kind of iron-based materials and species were studied for degradation refractory organic pollutants by visible light photo-Fenton method [24–30]. Based on previously reports, it can be summarized that iron minerals [26], iron oxide [25,30], iron composite oxides [29,31,32] and Fe(III) [24], single molecule iron complex [27,33] were combined with g-C_3N_4 photocatalysts for photocatalysis/photo-Fenton degradation of organic pollutants. α-FeOOH naturally exists in soils, sediments at the earth surface. Owing to its abundance and availability, relative stability and low cost, goethite has been widely used in environmental scavenger and water treatment.

In this paper, we choose FeOOH QDs as the iron containing Fenton

* Corresponding author.
E-mail address: yixin.zhao@sjtu.edu.cn (Y. Zhao).

https://doi.org/10.1016/j.apcatb.2018.05.074
Received 9 April 2018; Received in revised form 21 May 2018; Accepted 25 May 2018
Available online 31 May 2018
0926-3373/ © 2018 Elsevier B.V. All rights reserved.

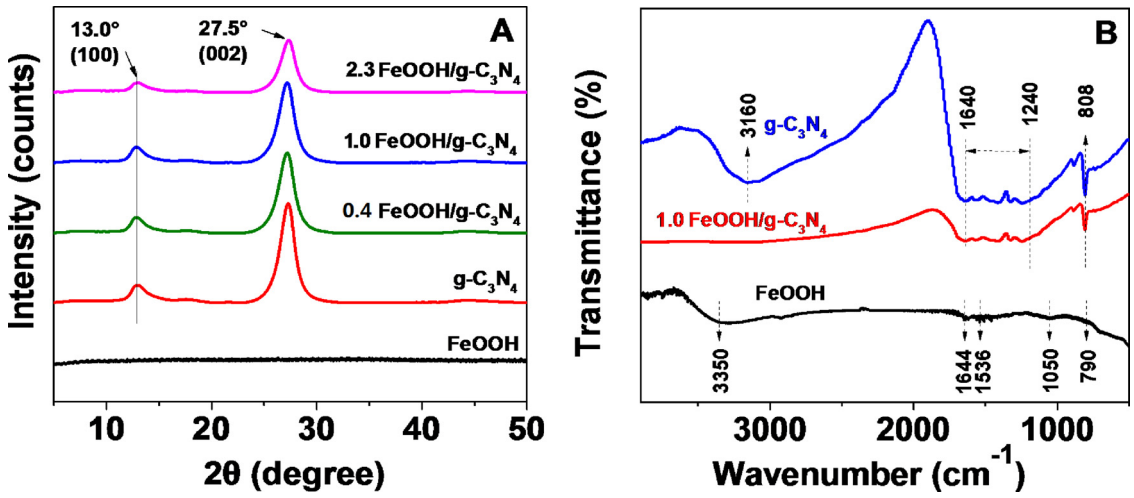

Fig. 1. Wide-angle XRD patterns (A) and FTIR spectra (B) of α-FeOOH QDs and the α-FeOOH coupled g-C_3N_4 composites.

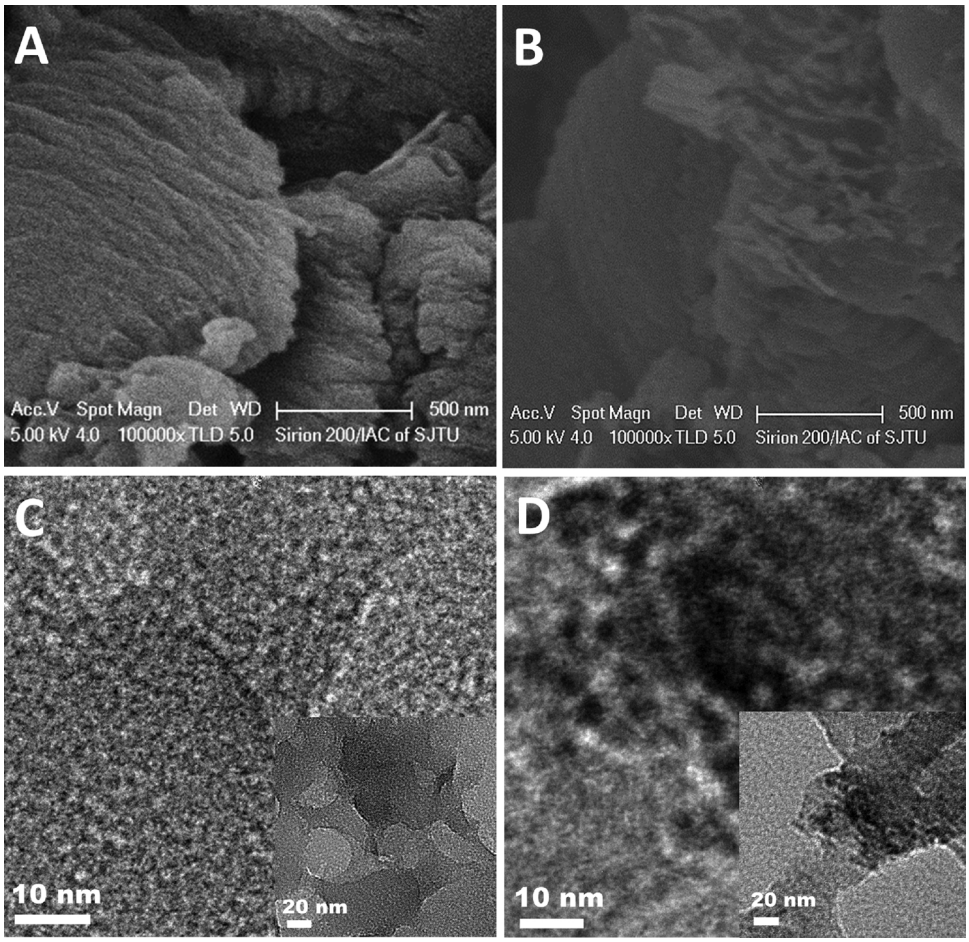

Fig. 2. SEM and TEM images of pure g-C_3N_4 (A, C) and FeOOH QDs coupled g-C_3N_4 (1.0Fe/g-C_3N_4) (B, D).

catalysts which were coupled with photocatalyst g-C_3N_4 to realize visible light driving photo-Fenton degrading and mineralization of organic pollutants. Under visible light irradiation, the FeOOH QDs showed negligible effect in photoelectron capture during the photocatalysis process of FeOOH QDs/g-C_3N_4 due to the amorphous nature of FeOOH QDs, but the visible light driving photo-Fenton degradation efficiency was greatly enhanced for FeOOH QDs/g-C_3N_4 attributing the interfacial electron transfer between FeOOH QDs and g-C_3N_4 via carbon species. The excited g-C_3N_4 photocatalyst generates electron and holes, the electron participated the reduction of iron (III) into iron (II) around the surface of FeOOH QDs. ROS scavenger experiment showed that ·OH radicals were the predominant oxidant in organic pollutants degradation. The FeOOH QDs coupled on g-C_3N_4 also showed high stability in recycling without iron leaching.

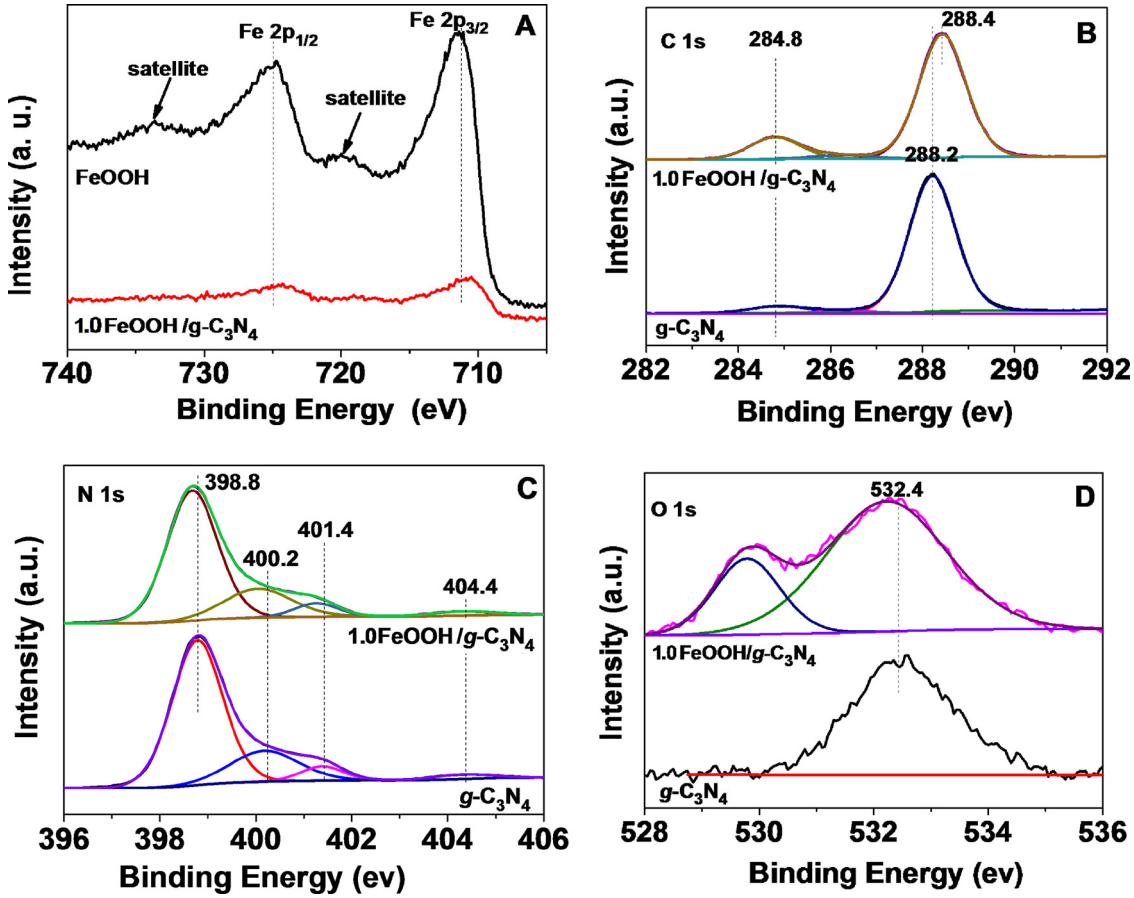

Fig. 3. High resolution spectra of Fe 2p (A), C 1 s (B) and N 1 s (C) and O 1 s (D) for different catalysts.

2. Experimental

2.1. Chemicals

Ferric chloride hexahydrate ($FeCl_3{\cdot}6H_2O$, 99.0%), ammonium bicarbonate (NH_4HCO_3, 21.0 ~ 22.0%), ethanol (C_2H_5OH, ≥99.7 wt%), tert-butyl alcohol ($C_4H_{10}O$, 98.0%), phenol (C_6H_5OH, ≥99.0 wt%), methyl orange ($C_{14}H_{14}N_3SO_3Na$, Mw = 327.33), EDTA ($C_{10}H_{14}N_2Na_2O_8{\cdot}2H_2O$, 99.0%) were purchased from Sinopharm Chemical Reagent Co., Ltd. Hydrogen peroxide (H_2O_2, 30%) was obtained from Shanghai Lingfeng Chemical Reagent Co., Ltd. All the aqueous solutions were prepared by using distilled water.

2.2. Materials synthesis

2.2.1. Synthesis of g-C_3N_4

g-C_3N_4 was synthesized by a fractional thermal polymerization method. Typically, 3.0 g of melamine was put into a crucible with a cover and heated from 20 °C to 520 °C at a heating rate of 4 °C/min. The heating treatment was kept at 520 °C for 4 h, and then the sample was naturally cooled down to room temperature. Subsequently, the resultant yellow agglomerate was milled into powder in a mortar and collected.

2.2.2. Synthesis of amorphous FeOOH-QDs/g-C_3N_4

The amorphous FeOOH-QDs/g-C_3N_4 was prepared according to a revised method [34]. Typically, 3 g of g-C_3N_4 was dissolved in different amounts of Ferric chloride hexahydrate - ethanol solution to obtain a mixture of 50 ml. After ultrasonic dispersion for 10 min, NH_4HCO_3 powder was added into the suspension with continuous stirring for 8 h. The prepared catalyst is designated as *x*FeOOH-QDs/g-C_3N_4 (*x* means the weight percentage of FeOOH) Pure amorphous FeOOH QDs were synthesized by the same method without addition of g-C_3N_4.

2.3. Characterization

X-ray diffraction (XRD) patterns were recorded on a Shimadzu XRD-6100 diffractometer with Cu Kα radiation. The data were recorded at a scan rate of 10/min. Fourier transform infrared (FT-IR) spectra were obtained on a Tensor 27 FTIR spectrometer (Nicolet 6700) with KBr as the reference sample. Field-emission scanning electron microscopy (FESEM) measurements and energy dispersive X-ray spectroscopy (EDX) were used to investigate the morphologies of the samples. Transmission electron microscopy (TEM) and high-resolution transmission electron microscopy (HRTEM) which were performed on a JEM-2100 F microscope. The UV–vis diffused reflectance spectra (DRS) of the as-synthesized samples were obtained from an UV–vis spectrophotometer (Lambda 750, PerkinElmer, UK). The iron content of the composite catalysts was determined by inductively coupled plasma optical emission spectrometer (ICP-AES, iCAP6300, Thermo). The lifetime of photo-excited charge carriers was recorded by time resolved photoluminescence spectroscopy (QM/TM/IM, PTI, USA).

2.4. Visible light induced photo-Fenton oxidation

Heterogeneous photo-Fenton oxidation of phenol and methylene orange (MO) was performed in dark and visible light irradiation for evaluating the catalytic activity of catalysts. Typically, 80 mg of catalyst was first mixed with 20 mL of aqueous phenol solution (50 mg L^{-1}) in a quartz flask irradiated by visible light and stirred for 30 min to achieve adsorption/desorption equilibrium of phenol. Then, 30 μL of H_2O_2 was added and the flask was sealed immediately. CO_2 were measured by a

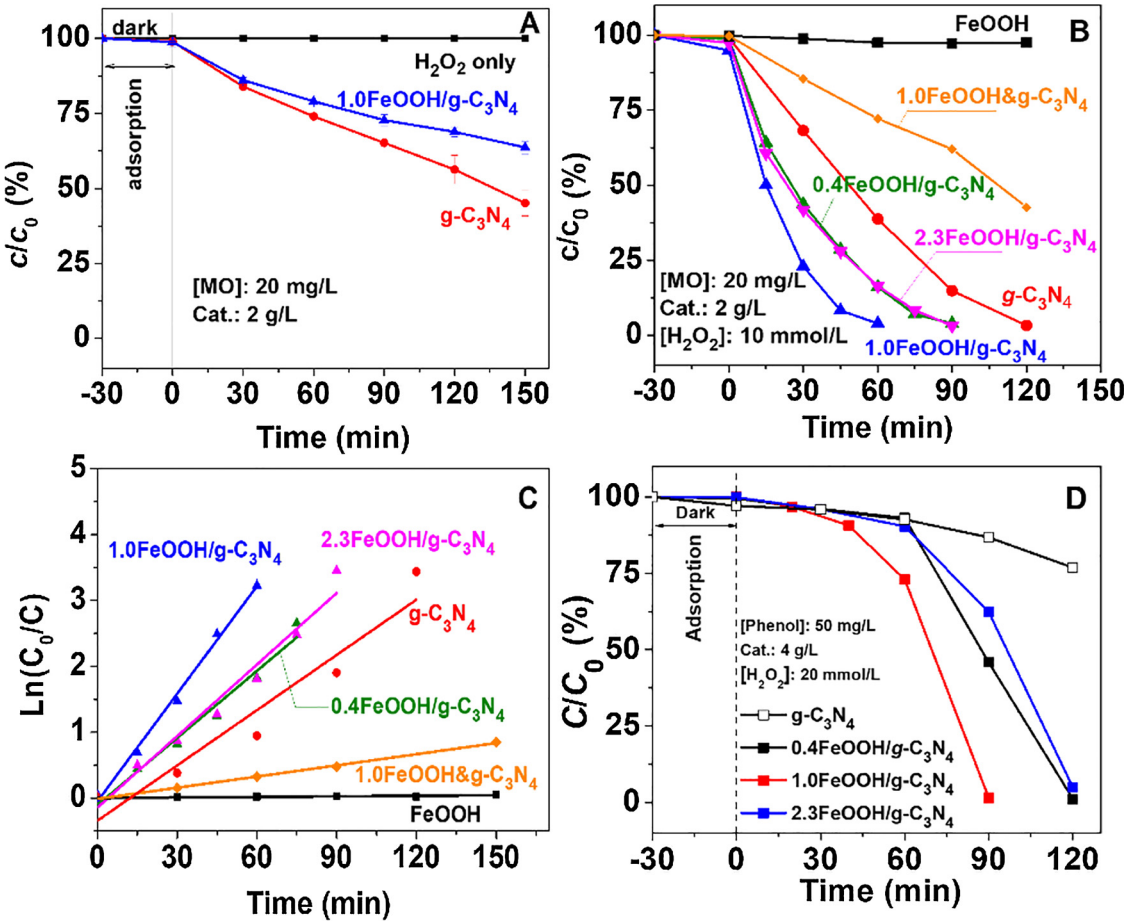

Fig. 4. Photocatalytic oxidation of MO (A); visible light driving photo-Fenton oxidation of MO on different catalysts (B); plot of L(c_0/c) vs. time (C); visible light driving photo-Fenton oxidation of phenol on different catalysts (D). Experimental conditions: initial pH of 5 and under visible light irradiation λ > 420 nm or in dark at 30 ± 3 °C.

gas chromatography (GC7900) for calculating the mineralization efficiency [21]. In order to exclude the temperature effect, the same procedure was performed in dark at 30–33 °C. A 500 W Xe lamp with a UV cutoff filter (> 420 nm) was used as the visible-light source. The MO concentration was analyzed by a UV–vis spectrophotometer (Cary 60, Agilent Technologies, US), and the absorbance wavelength was 464 nm. The stability of a catalyst was tested by repeatedly using the catalyst for five runs. After each catalytic reaction, the catalyst was separated, collected, washed with distilled water, and dried to be reused in the subsequent reaction cycle.

Cyclic voltammetry (CV) measurements were performed at 100 mV s^{-1} for each sample. Illumination of 100 mW/cm^2 was provided by a tungsten halogen lamp (CEL-TCH150, Ceaulight) as light source. All experiments were performed at ambient temperature (22 ± 2 °C) and electrode potentials were converted to the RHE scale using E(RHE) = E (Ag/AgCl) + 0.197 V + 0.059 × pH.

Quench reagent tert-butyl alcohol (TBA, 30 μL) was added into the supernatant before using liquid chromatography (LC-16, Shimadzu, Kyoto, Japan) to analyze the concentration of remaining phenol. Several trap agents including EDTA-2Na (10 mmol·L^{-1}) and tert-butyl alcohol (TBA, 30 mmol L^{-1}) were added into the model pollution solution to trap holes (h^+) and hydroxyl radicals (·OH). N_2 was pumped into the solution for 30 min before the reaction to detect superoxide radicals (·O_2^-).

3. Results and discussions

The physiochemical properties of FeOOH QDs coupled g-C_3N_4 were studied at first. Two distinct diffraction peaks appear at 13.0° (100) and 27.5° (002), corresponding to in-plane consecutive tri-s-thiazine motifs and the interlayer reflection of the graphitic like structure (Fig. 1A). With FeOOH QDs deposition, the diffraction peaks unchanged but the intensity gradually decreases with the increased amount of FeOOH QDs owing to its shield effect to X-ray.

FT-IR spectrum of the pure g-C_3N_4 MC shows a broad peak at 3000–3500 cm^{-1} ascribed to the stretching vibration of N—H and the stretching vibration of O—H of the physically adsorbed water (Fig. 1B). A serial of peaks in the range of 1240– 1640cm^{-1} can be assigned to the stretching vibration of C–N heterocycles [35]. The peak at 808 cm^{-1} is corresponding to the breathing mode of triazine units [36]. Normally the crystallized FeOOH QDs showed typical peak at 790 cm^{-1} corresponds to the flexural vibration of Fe—O—H, and 1050 cm^{-1}, 1536 cm^{-1} and 1644 cm^{-1} correspond to Fe-O vibration mode [37,38]. In the present case, the typical vibration mode of FeOOH QDs is not obvious in consistent with the literature indicating the high dispersion of amorphous FeOOH QDs [34,39].

The morphology of g-C_3N_4 keeps unchanged after the deposition of amorphous FeOOH QDs (Fig. 2A–B). The TEM image shows that FeOOH QDs are poorly crystallized (Fig. S1 and S2). The comparison of TEM images between pure g-C_3N_4 and 1.0Fe/g-C_3N_4 show that FeOOH QDs were coupled with g-C_3N_4 judging from the different contrast of FeOOH QDs and g-C_3N_4 (Fig. 2C, D). The EDX mapping showed that iron species were uniformly dispersed on the g-C_3N_4 (Fig. S3). The full spectrum of XPS for 1.0FeOOH/g-C_3N_4 shows the presence of elements C, N, O and Fe, respectively (Fig. S4). The Fe 2p spectra of pure FeOOH QDs and 1.0FeOOH/g-C_3N_4 were shown in Fig. 3A. Two well-resolved peaks

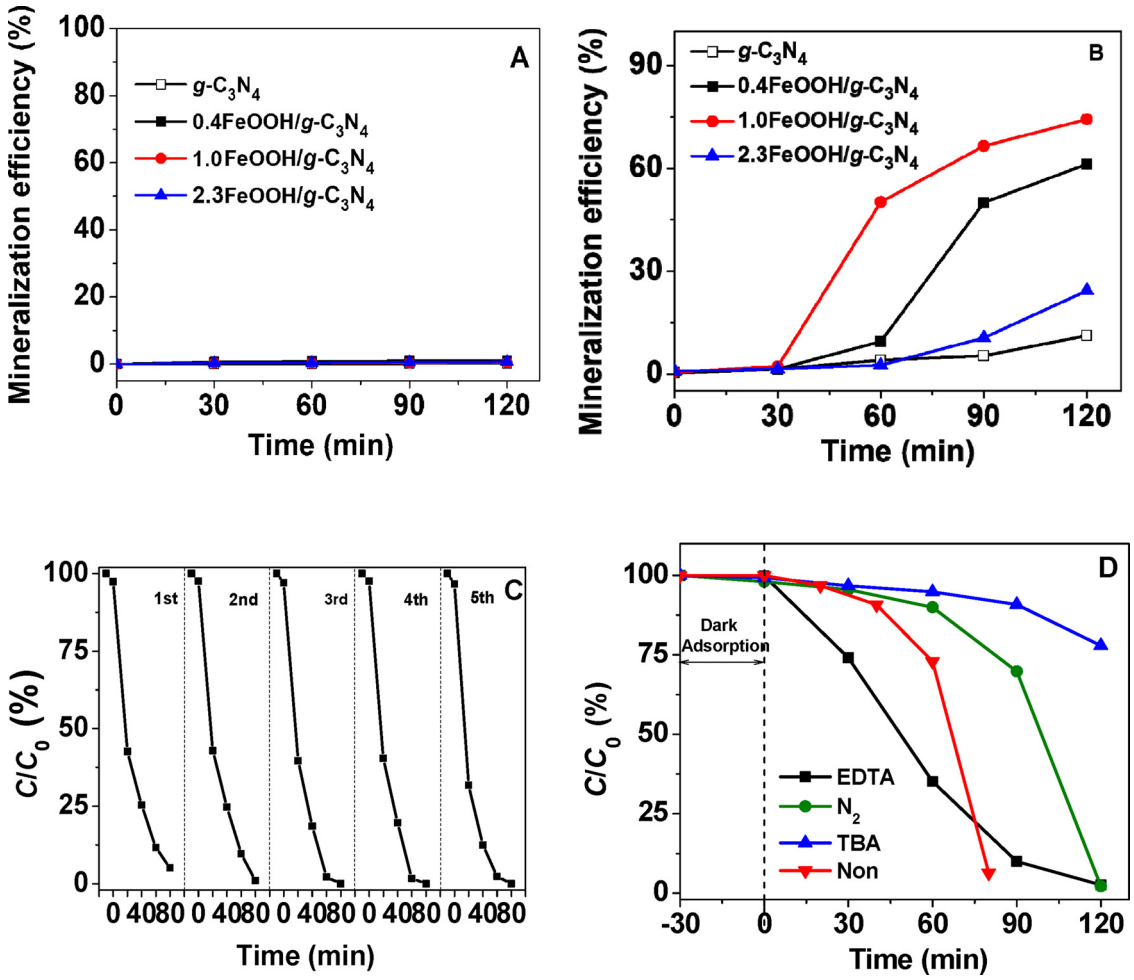

Fig. 5. Time profiles of phenol mineralization efficiencies in dark at 30 ± 3 °C (A) and visible light irradiation λ > 420 nm (B): 50 mg/L phenol, 4 g/L catalyst, 8 mmol H_2O_2; Cycling runs of visible light driving photo-Fenton degradation of MO on 1.0FeOOH/g-C_3N_4 (C): 25 mg/L MO, 2.0 g/L catalyst, initial pH 5, [H_2O_2] = 10 mmol/L; visible light driving photo-Fenton degradation of phenol with/without radical scavengers (D): 50 mg/L phenol, 4.0 g/L catalyst, initial pH 5, [H_2O_2] = 20 mmol/L.

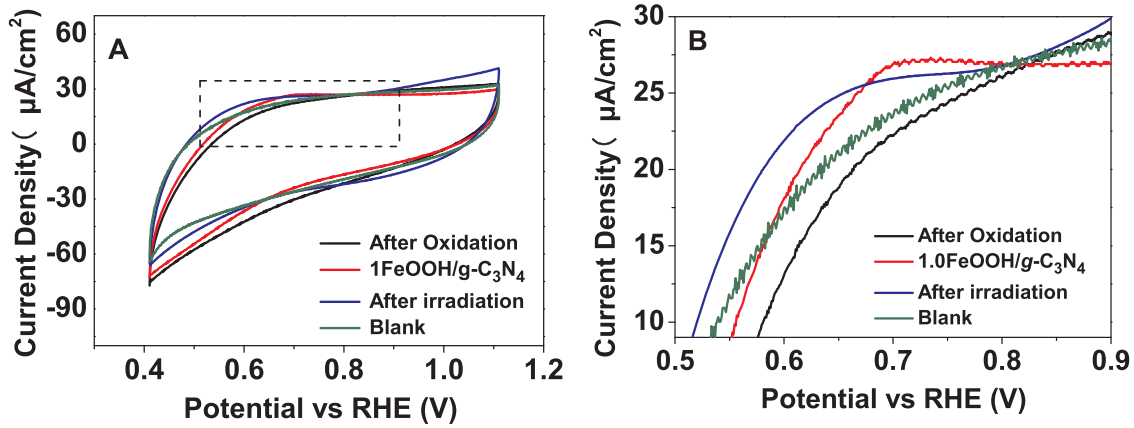

Fig. 6. Cyclic voltammograms of different electrodes at scan rate of 100 mV/s in 0.5 M Na_2SO_4 solution (pH = ~ 6) (A), the amplified CV curve in the potential range of 0.5 – 0.9 V at scan rate of 100 mV/s (B).

located at 710.9 eV and 725.0 eV were attributing to the Fe $2p_{3/2}$ and Fe $2p_{1/2}$, respectively, which indicates the formation of FeOOH. Two satellite peaks of Fe $2p_{3/2}$ and Fe $2p_{1/2}$ at 719.5 eV and 733.7 eV result from the charge transfer screening, which can be attributed to the presence of the Fe^{3+} ions of amorphous FeOOH QDs. For C 1s spectra of pure g-C_3N_4 and 1.0FeOOH/g-C_3N_4, the main peak at 288.4 eV corresponds to the sp^2-hybridized carbon in N–C=N triazine rings of the g-C_3N_4 (Fig. 3B). The peak at around 284.8 eV is identified as contaminated carbon. An obvious shift of C 1 s peak at 288.4 eV in the 1.0FeOOH/g-C_3N_4 compared with that of pure g-C_3N_4 (288.2 eV), indicating the chemical interaction between FeOOH QDs and g-C_3N_4. The intensified peaks at around 288.4 eV should be responsible for the

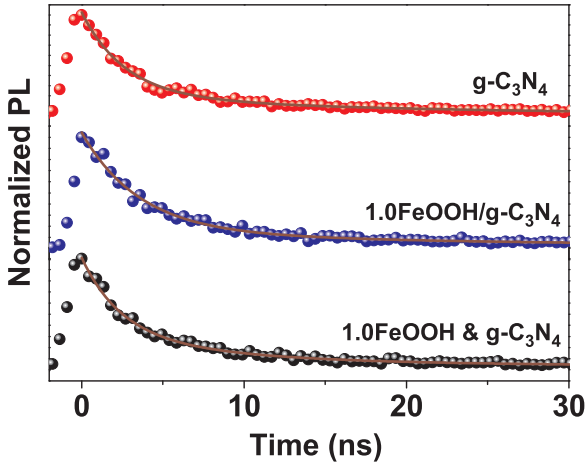

Fig. 7. Time-resolved PL decay curves of different materials.

Table 1
Parameters of time-resolved PL decay curves.

Materials	τ_1 (ns)	A_1	τ_2 (ns)	A_2	τ_{av} (ns)
g-C_3N_4	2.66	0.817	17.17	0.19309	11.42
1.0FeOOH/g-C_3N_4	3.54	0.89439	27.48	0.14373	16.82
1.0FeOOH&g-C_3N_4	2.40	0.30181	9.17	0.66755	8.45

formation of carbon species-C_3N_4 [40]. The N 1s spectra of pure g-C_3N_4 and 1.0FeOOH/g-C_3N_4 in Fig. 3C demonstrate typical N status in pyridinic (398.8 eV), pyrrolic (400.2 eV), amino functional groups (401.4 eV), and charging effects or positive charge localization in the heterocycles (404.3 eV), respectively [36]. The O 1s spectra shows a peak at 532.06 eV on pure g-C_3N_4 owing to the adsorbed H_2O, and an additional peak at 529.8 eV assigning to the Fe—O—Fe and Fe—OH on 1.0FeOOH/g-C_3N_4 (Fig. 3D).

The photocatalytic and photo-Fenton performance was measured. The MO was very stable under visible light irradiation even with H_2O_2 (Fig.4A). The photocatalytic decolorization efficiency of MO on 1.0FeOOH/g-C_3N_4 was lower than that on pure g-C_3N_4 which indicates that the deposition of amorphous FeOOH QDs may shield the active sites of pure g-C_3N_4 (Fig.4A). The photocatalytic efficiencies of pure g-C_3N_4 and 1.0FeOOH/g-C_3N_4 were low and the amorphous FeOOH QDs show negative effect on photogenerated charges separation which acted as the electron acceptor in some case [40].

Previous result has reported that pure g-C_3N_4 possessed photo-Fenton activity to catalyze H_2O_2 under visible light irradiation excitation [22], wherein photogenerated e^- participates the production of $OH\cdot$ as follows:

$$g\text{-}C_3N_4 \xrightarrow{Vis.} g\text{-}C_3N_4(e^-, h^+) \quad (1)$$

$$H_2O_2 + e^- \rightarrow OH^- + OH\cdot \quad (2)$$

In the present study, we deposited FeOOH QDs on g-C_3N_4 and served in photo- Fenton degradation of organic pollutants. The visible light driving photo-Fenton performances of different catalysts were measured (Fig. 4B). As shown in Fig. 4A, the MO was hardly removed by H_2O_2-only under visible light irradiation indicating the chemical stability of MO in the presence of H_2O_2 and visible light. For FeOOH QDs coupled g-C_3N_4, photo-Fenton decolorization efficiency reached ~ 100% after 60 min, 90 min and 120 min under visible light irradiation for 1.0FeOOH/g-C_3N_4, 0.4FeOOH/g-C_3N_4 (2.3FeOOH/g-C_3N_4) and pure g-C_3N_4, respectively. It should be mentioned that the decolorization efficiency only reached 60% after 120 min for the mixture 1.0FeOOH& g-C_3N_4. The mixture and pure g-C_3N_4 showed the relative low photo-Fenton decolorization efficiency with visible light irradiation, which implies that the FeOOH QDs coupled on g-C_3N_4 are more active than the pure g-C_3N_4 and the mixture. Pure amorphous FeOOH QDs is nearly inactive under the same condition. The visible light driving photo-Fenton decolorization of MO conforms to pseuso-first-order kinetic model. The highest rate constant achieves 0.054 min^{-1} for 1.0FeOOH/g-C_3N_4 which is nearly 10 times higher than that of the mixture (0.0057 min^{-1}), 2 times than those of pure g-C_3N_4 (0.031 min^{-1}), 0.4FeOOH/g-C_3N_4 (0.034 min^{-1}) and 2.3FeOOH/g-C_3N_4 (0.036 min^{-1}), respectively (Fig. 4C). The above phenomena indicate that the coupling interface between FeOOH QDs and g-C_3N_4 is a decisive factor. The proper amount and high dispersion of FeOOH QDs can not only provide more coupling interfaces which are the active sites for degradation of pollutants, but also show less negative effects on light absorption of g-C_3N_4.

The visible light driving photo-Fenton oxidation of phenol was measured on different catalysts. As shown in Fig. 4D, phenol was completely oxidized after 90 min on 1.0FeOOH/g-C_3N_4. For both of 0.4FeOOH/g-C_3N_4 and 2.3FeOOH/g-C_3N_4, phenol was oxidized after about 120 min. The phenol oxidation efficiency of pure g-C_3N_4 is obviously lower than those of the FeOOH QDs coupled g-C_3N_4. The phenomenon is in good agreement with the MO decolorization (Fig. 4A). The above results also indicate that the photo-activation of g-C_3N_4 is essential for the photo-Fenton oxidation and the synergistic effect between FeOOH QDs and g-C_3N_4 should be very crucial for visible light assisted photo-Fenton degradation of organic pollutants.

The mineralization efficiencies for various catalysts were performed in dark and visible light conditions. As shown in Fig.5A, phenol was hardly mineralized in dark for both of pure g-C_3N_4 and FeOOH QDs coupled g-C_3N_4. The results reflect that oxidation potential was very low for g-C_3N_4 without visible light activation and the FeOOH QDs are also unable to catalyze H_2O_2 and mineralize phenol in dark. Under visible light irradiation, phenol was not completely mineralized into

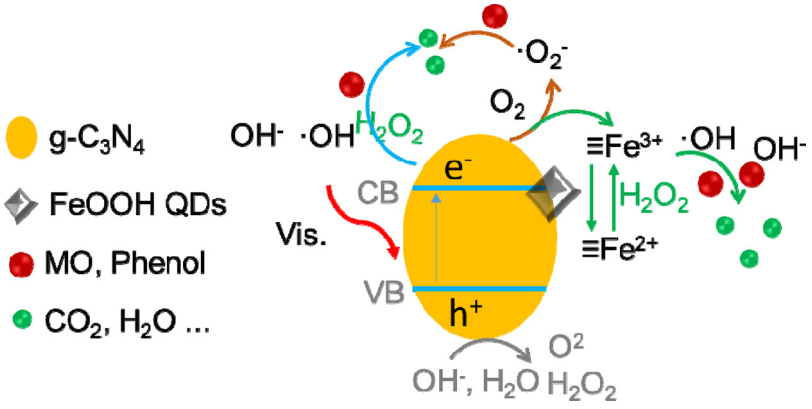

Scheme 1. A schematic illustration of visible light driving photo-Fenton oxidation of organic pollutants over FeOOH QDs coupled g-C_3N_4.

CO_2 within the first 30 min for all of the catalysts, and then the mineralization efficiency of phenol increased gradually (Fig. 5B). At first 30 min, most of the phenol rings were opened and oxidized into organic acid before being completely mineralized (data not shown here). The mineralization efficiencies in 2-h reached 61%, 74% and 24% for 0.4FeOOH/*g*-C_3N_4, 1.0FeOOH/*g*-C_3N_4 and 2.3FeOOH/*g*-C_3N_4, respectively. The most efficient 1.0FeOOH/*g*-C_3N_4 is nearly 7 times than the pure *g*-C_3N_4 (11%), which indicates that FeOOH coupled on *g*-C_3N_4 has the promising potential for deep treatment of recalcitrant organic pollutants.

To investigate the stability and reusability of FeOOH QDs coupled *g*-C_3N_4, the reused 1.0FeOOH/*g*-C_3N_4 was washed with distilled water, dried in vacuum and then reused four times for phenol degradation under visible light irradiation. As observed in Fig. 5C, the removal efficiency of MO in five cycles all reached to 100% within 80 min, and the degradation rate increased slightly and kept stable from the third run to the fifth run, which implies the activation phenomenon of catalysts during the visible light driving photo-Fenton oxidation of MO. The soluble iron ion concentrations in solution after each run were measured, but it was not detectable for each of the run. The phenomenon indicates that the Fe(II)/F(III) cycling proceeded on the surface of 1.0FeOOH/*g*-C_3N_4.

In order to check the active species in the photo-Fenton process, different scavengers were used to capture the different radicals. As shown in Fig. 5D, the photo- Fenton performance decayed greatly in the presence of TBA which can quench the OH· radicals. In the N_2 (O^{2-}·- scavenger) bubbled phenol solution, the degradation efficiency also decreased which indicate that OH· and O^{2-}· radicals contribute the degradation of phenol. With the addition of h^+ scavenger EDTA, the degradation efficiency increased at first and then decreased which should be caused by the enhanced separation of photogenerated e^-/h^+ pairs by consuming h^+. It also reflects that the photogenerated e^- is more valid than h^+ during the visible light driving photo-Fenton process.The cyclic voltammogram curves show rectangular shapes at scan rate of 100 mV/s (Fig. 6A). An oxidative peak appears at 0.6–0.7 V for 1.0FeOOH/*g*-C_3N_4 modified electrode indicating the oxidation of Fe(II) in 1.0FeOOH/*g*-C_3N_4 (Fig. 6B). Based on the above results, Fe(II) species was present in 1.0FeOOH/*g*-C_3N_4 [41]. The CV curve of 1.0FeOOH/*g*-C_3N_4 electrode treated with high potential (after oxidation) shows negligible oxidation peaks which appears again after light irradiation (Fig. 6B). The phenomenon probably reflects the transformation of Fe(III) to Fe(II) under visible light irradiation.

Owing to the higher formation potential (1.99 eV vs. NHE) of OH·/OH^- than the VB potential of pure *g*-C_3N_4, it can hardly produce OH· under visible light irradiation. Accordingly, it is sure that the OH· radicals were generated in another pathway. Based on the results of photo-Fenton degradation of MO, the FeOOH QDs coupled on *g*-C_3N_4 can effectively enhance the visible light driving photo-Fenton degradation efficiency, while the pure FeOOH QDs aggregates is inactive in dark condition. FeOOH QDs coupled *g*-C_3N_4 showed negative effect on photocatalytic decolorization of MO without H_2O_2 which should be caused by the amorphous nature of FeOOH QDs. However, in the presence of H_2O_2, the excitation of *g*-C_3N_4 combined with the FeOOH QDs promotes the production of OH· (Fig. 5D). According to the XPS results, we found that carbon species was present with the deposition of FeOOH QDs. In order to measure the transferring of photo-excited charges, we recorded the emission lifetime by time-resolved PL instrumentation on pure *g*-C_3N_4, composite FeOOH/*g*-C_3N_4 and mixture FeOOH&*g*-C_3N_4, respectively (Fig. 7). A two-exponential function equation was fitted to the data on the PL decay profile. Decay times (τ_1 and τ_2) and PL aptitudes (A_1 and A_2) were present in Table 1. From Fig. 7 and Table 1, it was found that the average lifetime (τ_{av}) of the photo-excited charges in the 1.0FeOOH/*g*-C_3N_4 composite is 11.8 ns which is higher than those of pure *g*-C_3N_4 (11.4 ns) and the mixture FeOOH&*g*-C_3N_4 (6.7 ns). The increase in the photoluminescence lifetime implies the decrease in radiative recombination [42]. The photo-excited electrons or holes with a longer lifetime on the surface are benefit for the cycling of Fe(III)/Fe(II). The photoexcited e^- should transfer from VB of *g*-C_3N_4 to interfacial Fe(III) via conductive carbon species which reduced Fe(III) into Fe(II) (Fe(III)/Fe(II), 0.77 V, vs NHE). Surface Fe(II) efficiently activate the H_2O_2 to produce OH· and then it is oxidized to Fe(III) (Scheme 1). Normally, the transformation from Fe(III) to Fe(II) is the decisive step for Fenton reaction, the efficient reduction of Fe(III) to Fe(II) can enhance the utilization efficiency of H_2O_2. Additionally, the carbon species interacted with FeOOH QDs among FeOOH QDs and *g*-C_3N_4 was responsible for the iron leaching problem. We think that the e^- transferring with long lifetime occurs at the interface of FeOOH/*g*-C_3N_4 via carbon species while it also contributes the confinement of Fe ions. Besides the main photo-Fenton path way to produce OH·, the photo-excited e^- also can be captured by O_2 to form $\cdot O_2^-$ radicals.

4. Conclusions

In this study, we reported a visible light driving photo-Fenton catalyst in which amorphous FeOOH QDs coupled with *g*-C_3N_4. The interfacial electron transfer between *g*-C_3N_4 and FeOOH QDs in the presence of carbon species induced the high efficiency on degradation and mineralization of organic pollutants by visible light driving photo-Fenton process. The ·OH radicals were proved to be the predominant oxidants and O^{2-} radicals were also contributors in the above process. The iron leaching was as low as detection limit during the recycling test which showed high stability during the visible light driving photo-Fenton oxidation process. The combination of *g*-C_3N_4 with FeOOH QDs is very necessary for interfacial electron transfer and the carbon species contribute the Fe ions confinement. It is a promising visible light driving photo-Fenton catalyst for treating recalcitrant organic waste water.

Acknowledgements

This work is supported by National Natural Science Foundation of China (21777097, 21507083, 21777096), Key Laboratory of International Joint Laboratory of Resource Chemistry (IJLRC), Ministry of Education and Opening Project of Key Laboratory of Green Chemistry of Sichuan Institutes of Higher Education (LZJ1704).

Appendix A. Supplementary data

Supplementary material related to this article can be found, in the online version, at doi:https://doi.org/10.1016/j.apcatb.2018.05.074.

References

[1] X.F. Qian, K. Fuku, Y. Kuwahara, T. Kamegawa, K. Mori, H. Yamashita, Design and functionalization of photocatalytic systems within mesoporous silica, ChemSusChem 7 (2014) 1528–1536.
[2] A.R. Ribeiro, O.C. Nunes, M.F.R. Pereira, A.M.T. Silva, An overview on the advanced oxidation processes applied for the treatment of water pollutants defined in the recently launched directive 2013/39/EU, Environ. Int. 75 (2015) 33–51.
[3] S. Wang, A comparative study of Fenton and Fenton-like reaction kinetics in decolourisation of wastewater, Dyes Pigm. 76 (2008) 714–720.
[4] C. Black, Veatch, Advanced Oxidation Processes, White's Handbook of Chlorination and Alternative Disinfectants, John Wiley & Sons, Inc., 2010, pp. 976–1002.
[5] M. Hartmann, S. Kullmann, H. Keller, Wastewater treatment with heterogeneous Fenton-type catalysts based on porous materials, J. Mater. Chem. 20 (2010) 9002–9017.
[6] M. Ocampo-Gaspar, C.F. Cano-Guzman, L.F. Payan-Martinez, L. Gonzalez-Reyes, I. Hernandez-Perez, V. Garibay-Febles, J.P. Perez-Orozco, L.I. Cabrera-Lara, M.L. Ramon-Garcia, L. Galicia-Luis, R. Suarez-Parra, Sizing the Fenton's catalyst, J. Photochem. Photobiol. A-Chem. 353 (2018) 527–535.
[7] S. Navalon, M. Alvaro, H. Garcia, Heterogeneous Fenton catalysts based on clays, silicas and zeolites, Appl. Catal. B-Environ. 99 (2010) 1–26.
[8] X.G. Duan, Z.M. Ao, H.Q. Sun, S. Indrawirawan, Y.X. Wang, J. Kang, F.L. Liang, Z.H. Zhu, S.B. Wang, Nitrogen-doped graphene for generation and evolution of reactive radicals by metal-free catalysis, ACS Appl. Mater. Interfaces 7 (2015) 4169–4178.
[9] M. Cheng, G. Zeng, D. Huang, C. Lai, P. Xu, C. Zhang, Y. Liu, Hydroxyl radicals

based advanced oxidation processes (AOPs) for remediation of soils contaminated with organic compounds: a review, Chem. Eng. J. 284 (2016) 582–598.
[10] Y. Qin, L. Zhang, T. An, hydrothermal carbon-mediated Fenton-like reaction mechanism in the degradation of alachlor: direct electron transfer from hydrothermal carbon to Fe(III), ACS Appl. Mater. Interfaces 9 (2017) 17116–17125.
[11] H. Huang, S. Tu, C. Zeng, T. Zhang, A.H. Reshak, Y. Zhang, Macroscopic polarizaiton enhancement promoting photo- and piezoelectric-induced charge seperation and molecular oxygen, Angew. Chem. Int. Ed. 56 (2017) 11860–11864.
[12] H. Li, J. Shang, Z. Yang, W. Shen, Z. Ai, L. Zhang, Oxygen vacancy associated surface Fenton chemistry: surface structure dependent hydroxyl radicals generation and substrate dependent reactivity, Environ. Sci. Technol. 51 (2017) 5685–5694.
[13] H. Chen, Z. Zhang, Z. Yang, Q. Yang, B. Li, Z. Bai, Heterogeneous Fenton-like catalytic degradation of 2,4-dichlorophenoxyacetic acid in water with FeS, Chem. Eng. J. 273 (2015) 481–489.
[14] H. Lan, A. Wang, R. Liu, H. Liu, J. Qu, Heterogeneous photo-Fenton degradation of acid red B over Fe2O3 supported on activated carbon fiber, J. Hazard. Mater. 285 (2015) 167–172.
[15] R. Li, X. Jin, M. Megharaj, R. Naidu, Z. Chen, Heterogeneous Fenton oxidation of 2,4-dichlorophenol using iron-based nanoparticles and persulfate system, Chem. Eng. J. 264 (2015) 587–594.
[16] M. Munoz, Z.M. de Pedro, J.A. Casas, J.J. Rodriguez, Preparation of magnetite-based catalysts and their application in heterogeneous Fenton oxidation – a review, Appl. Catal. B-Environ. 176 (2015) 249–265.
[17] Y. Feng, D. Wu, Y. Deng, T. Zhang, K. Shih, Sulfate radical-mediated degradation of sulfadiazine by CuFeO2 rhombohedral crystal-catalyzed peroxymonosulfate: synergistic effects and mechanisms, Environ. Sci. Technol. 50 (2016) 3119–3127.
[18] X. Hou, X. Huang, Z. Ai, J. Zhao, L. Zhang, Ascorbic acid/Fe@Fe2O3: a highly efficient combined Fenton reagent to remove organic contaminants, J. Hazard. Mater. 310 (2016) 170–178.
[19] F. Xiao, W. Li, L. Fang, D. Wang, Synthesis of akageneite (beta-FeOOH)/reduced graphene oxide nanocomposites for oxidative decomposition of 2-chlorophenol by fenton-like reaction, J. Hazard. Mater. 308 (2016) 11–20.
[20] W.J. Song, M.M. Cheng, J.H. Ma, W.H. Ma, C.C. Chen, J.C. Zhao, Decomposition of hydrogen peroxide driven by photochemical cycling of iron species in clay, Environ. Sci. Technol. 40 (2006) 4782–4787.
[21] X. Qian, M. Ren, Y. Zhu, D. Yue, Y. Han, J. Jia, Y. Zhao, Visible light assisted heterogeneous Fenton-like degradation of organic pollutant via alpha-FeOOH/mesoporous carbon composites, Environ. Sci. Technol. 51 (2017) 3993–4000.
[22] H. Huang, K. Xiao, N. Tian, F. Dong, T. Zhang, X. Du, Y. Zhang, Template-free precursor-surface-etching route to porous, thin g-C3N4 nanosheet for enhancing photocatalytic reduction and oxidation activity, J. Mater. Chem. A 5 (2017) 17452–17463.
[23] Y. Cui, Z. Ding, P. Liu, M. Antonietti, X. Fu, X. Wang, Metal-free activation of H2O2 by g-C3N4 under visible light irradiation for the degradation of organic pollutants, Phys. Chem. Chem. Phys. 14 (2012) 1455–1462.
[24] J.-Y. Hu, K. Tian, H. Jiang, Improvement of phenol photodegradation efficiency by a combined g-C3N4/Fe(III)/persulfate system, Chemosphere 148 (2016) 34–40.
[25] L. Zhou, L. Wang, J. Zhang, J. Lei, Y. Liu, Well-dispersed Fe2O3 nanoparticles on g-C3N4 for efficient and stable photo-fenton photocatalysis under visible-light irradiation, Eur. J. Inorg. Chem. (2016) 5387–5392.
[26] D. He, Y. Chen, Y. Situ, L. Zhong, H. Huang, Synthesis of ternary g-C3N4/Ag/gamma-FeOOH photocatalyst: an integrated heterogeneous Fenton-like system for effectively degradation of azo dye methyl orange under visible light, Appl. Surf. Sci. 425 (2017) 862–872.
[27] X. Li, Y. Pi, L. Wu, Q. Xia, J. Wu, Z. Li, J. Xiao, Facilitation of the visible light-induced Fenton-like excitation of H2O2 via heterojunction of g-C3N4/NH2-iron terephthalate metal-organic framework for MB degradation, Appl. Catal. B-Environ. 202 (2017) 653–663.
[28] J. Ma, Q. Yang, Y. Wen, W. Liu, Fe-g-C3N4/graphitized mesoporous carbon composite as an effective Fenton-like catalyst in a wide pH range, Appl. Catal. B-Environ. 201 (2017) 232–240.
[29] X. Wang, A. Wang, J. Ma, Visible-light-driven photocatalytic removal of antibiotics by newly designed C3N4@MnFe2O4-graphene nanocomposites, J. Hazard. Mater. 336 (2017) 81–92.
[30] Z. Wang, Y. Fan, R. Wu, Y. Huo, H. Wu, F. Wang, X. Xu, Novel magnetic g-C3N4/alpha-Fe2O3/Fe3O4 composite for the very effective visible-light-Fenton degradation of orange II, RSC Adv. 8 (2018) 5180–5188.
[31] Y. Yao, Y. Cai, F. Lu, J. Qin, F. Wei, C. Xu, S. Wang, Magnetic ZnFe2O4-C3N4 hybrid for photocatalytic degradation of aqueous organic pollutants by visible light, Ind. Eng. Chem. Res. 53 (2014) 17294–17302.
[32] Y. Yao, F. Lu, Y. Zhu, F. Wei, X. Liu, C. Lian, S. Wang, Magnetic core-shell CuFe2O4@C3N4 hybrids for visible light photocatalysis of Orange II, J. Hazard. Mater. 297 (2015) 224–233.
[33] K.-Y.A. Lin, J.-T. Lin, Ferrocene-functionalized graphitic carbon nitride as an enhanced heterogeneous catalyst of Fenton reaction for degradation of rhodamine B under visible light irradiation, Chemosphere 182 (2017) 54–64.
[34] J.Q. Liu, M.B. Zheng, X.Q. Shi, H.B. Zeng, H. Xia, Amorphous FeOOH quantum dots assembled mesoporous film anchored on graphene nanosheets with superior electrochemical performance for supercapacitors, Adv. Funct. Mater. 26 (2016) 919–930.
[35] M. Xu, L. Han, S. Dong, Facile fabrication of highly efficient g-C3N4/Ag2O heterostructured photocatalysts with enhanced visible-light photocatalytic activity, ACS Appl. Mater. Interfaces 5 (2013) 12533–12540.
[36] H.C. Yang, S.W. Zhang, R.Y. Cao, X.L. Deng, Z.P. Li, X.J. Xu, Constructing the novel ultrafine amorphous iron oxyhydroxide/g-C3N4 nanosheets heterojunctions for highly improved photocatalytic performance, Sci. Rep. 7 (2017) 12.
[37] J.F. Banfield, S.A. Welch, H.Z. Zhang, T.T. Ebert, R.L. Penn, Aggregation-based crystal growth and microstructure development in natural iron oxyhydroxide biomineralization products, Science 289 (2000) 751–754.
[38] R.L. Penn, J.J. Erbs, D.M. Gulliver, Controlled growth of alpha-FeOOH nanorods by exploiting-oriented aggregation, J. Cryst. Growth 293 (2006) 1–4.
[39] Z. Zhu, Z. Lu, D. Wang, X. Tang, Y. Yan, W. Shi, Y. Wang, N. Gao, X. Yao, H. Dong, Construction of high-dispersed Ag/Fe3O4/g-C3N4 photocatalyst by selective photodeposition and improved photocatalytic activity, Appl. Catal. B-Environ. 182 (2016) 115–122.
[40] Y. Li, H. Zhang, P. Liu, D. Wang, Y. Li, H. Zhao, Cross-linked g-C3N4/rGO nanocomposites with tunable band structure and enhanced visible light photocatalytic activity, Small 9 (2013) 3336–3344.
[41] N. Panda, H. Sahoo, S. Mohapatra, Decolourization of methyl orange using Fenton-like mesoporous Fe2O3-SiO2 composite, J. Hazard. Mater. 185 (2011) 359–365.
[42] X. Xu, F. Zhang, S. Xu, J. He, L. Wang, D.G. Evans, X. Duan, Chem. Commun. (2009) 7533–7535.